أكاديمية كاوست
KAUST ACADEMY

جامعة الملك عبدالله
للعلوم والتقنية
King Abdullah University of
Science and Technology

Hydrogen Mixing and Recovery in Subsurface Storage During Repeated Injection–Withdrawal Cycles

Abdulhakeem Alduaij, Prof. Andy Woods

abdulhakeem.alduaij@kaust.edu.sa, aww1@cam.ac.uk

Abstract

This project investigates the mixing and spatial distribution of hydrogen during repeated injection–withdrawal cycles in a laboratory-scale model of subsurface hydrogen storage. Image-based analysis is used to quantify the evolution of the hydrogen plume and concentration distribution throughout the storage cycles, with particular focus on the development of the mixing zone. The objective is to understand how repeated injection and withdrawal influence hydrogen mixing and ultimately provide insight into hydrogen recovery and during subsurface storage.

Date: August 24, 2026

Contents

1 Introduction **3**

1.1 Background . . . 3
1.2 Problem Statement . . . 3
1.3 Objectives . . . 3
1.4 Scope and Assumptions . . . 4

2 Related Work **4**

2.1 Underground Hydrogen Storage . . . 4
2.2 Hydrogen Transport and Mixing . . . 4
2.3 Effect of Operating Conditions . . . 5
2.4 Research Gap . . . 5

3 Methodology **5**

3.1 Experimental Overview . . . 5
3.2 Experimental Data and Cycle Definition . . . 6
3.3 Radial Concentration Analysis . . . 6
3.4 Effective Radius . . . 6
3.5 Mixing-Zone Thickness . . . 7
3.6 Mixing-Zone Area . . . 7
3.7 Hydrogen Recovery . . . 8
3.8 Plume Expansion Rate . . . 8
3.9 Estimated Equivalent Injection Flow Rate . . . 8
3.10 Comparison Procedure . . . 9
3.11 Data Processing and Computational Tools . . . 9

4 Results **10**

4.1 Overview of Experimental Results . . . 10
4.2 Effective Radius . . . 10
4.3 Integrated Normalized Hydrogen Content . . . 11
4.4 Hydrogen Recovery . . . 12
4.5 Mixing-Zone Thickness . . . 13
4.6 Mixing-Zone Area . . . 13
4.7 Relationship Between Mixing-Zone Thickness and Effective Radius . . . 15
4.8 Relationship Between Mixing-Zone Area and Effective Radius . . . 16
4.9 Plume Expansion Rate . . . 16
4.10 Estimated Equivalent Injection Flow Rate . . . 17
4.11 Overall Comparison of Injection Conditions . . . 18

5 Discussion **19**

5.1 Effect of Injection Rate on Plume Development . . . 19
5.2 Plume Size and Hydrogen Accumulation . . . 20
5.3 Behaviour of the Mixing Zone . . . 20
5.4 Hydrogen Recovery During Repeated Cycling . . . 21

5.5 Plume Expansion Rate 21
5.6 Injection and Withdrawal Behaviour 22
5.7 Implications of the Experimental Comparison 22

6 Limitations and Future Work **22**
6.1 Limitations 22
6.2 Future Work 23

7 Conclusion **24**

References **25**

1 Introduction

1.1 Background

Hydrogen has become widely considered as an energy carrier that could facilitate the transition towards lower-carbon energy systems [1]. Its importance in the context of renewable energy integration arises from the ability to produce hydrogen using electricity during periods of high renewable generation and subsequently store it for use during periods of high energy demand. However, the large-scale implementation of hydrogen systems requires storage technologies capable of accommodating substantial quantities of hydrogen over extended periods.

Underground hydrogen storage (UHS) has recently been proposed as a potential option for large-scale and long-term storage of hydrogen [1, 2]. Hydrogen can be stored in geological formations such as salt caverns, depleted oil and gas reservoirs, and deep saline aquifers [1, 2]. In UHS, hydrogen is injected into the geological formation and subsequently withdrawn, typically through repeated cycles of injection and withdrawal [1, 3]. For such a process to operate effectively, hydrogen transport, mixing, and recovery are important factors in addition to storage capacity.

It is therefore important to consider hydrogen transport and mixing because processes such as diffusion, capillary trapping, and other multiphase-flow mechanisms can affect hydrogen recovery and storage performance [1, 3]. Moreover, the injection rate and the number of injection–withdrawal cycles may influence the development of the hydrogen plume and its recovery during repeated cycling [3].

1.2 Problem Statement

Spatial pattern of hydrogen concentration for both injection and withdrawal is dynamic. As a result, characterization of storage performances through hydrogen concentration is not sufficient; plume behavior and the mixing zone should also be taken into account. Nevertheless, it is not clear how the effect of injection rate influences plume growth, mixing zone formation, integrated hydrogen content, and hydrogen recovery from the experimental data obtained in this work. That is why this work aims at investigating experimental radial hydrogen concentration profiles under various injection rates. Quantification of effective plume radius, mixing zone thickness, mixing zone area, integrated normalized hydrogen content, and hydrogen recovery is done.

The radial hydrogen concentration profiles are obtained from experimental radial light-intensity distributions. No calibration curve between light intensity and hydrogen concentration was developed, and thus the concentration values used in the work should be considered as normalized concentrations rather than absolute. The integrated hydrogen content used in this analysis is radially integrated concentration signal, not an absolute hydrogen mass.

1.3 Objectives

The main objectives of this study are:

1. To investigate the effect of hydrogen injection rate on plume expansion during cyclic injection and withdrawal.
2. To quantify the evolution of the effective plume radius, mixing-zone thickness, and mixing-zone area over repeated cycles.
3. To evaluate hydrogen accumulation and recovery during repeated injection and withdrawal.
4. To compare plume evolution, mixing behavior, hydrogen accumulation, and recovery between fast, intermediate, and slow injection conditions.

1.4 Scope and Assumptions

The concentration profiles are deduced from experimental radial distributions of light intensities, which have been normalized to obtain normalized concentrations. No calibration relationship between the light intensity and the absolute concentration of hydrogen was created. Thus, the concentration data, which are considered in this paper, are regarded as normalized concentrations rather than absolute concentrations. Accordingly, the radially integrated hydrogen content analyzed here is radially integrated concentration signal, but not an absolute mass of hydrogen.

Three injection scenarios, fast, intermediate and slow ones, are studied in the present paper. Each cycle is composed of 30 seconds of injection and 30 seconds of withdrawal. The effective radius and properties of mixing zone are evaluated using the experimental radial concentration profile. The equivalent flow rate of injection is determined from the difference of integrated normalized hydrogen contents at the end of the previous stage of withdrawal and at the end of the current injection stage, considering the thickness of experiments.

2 Related Work

2.1 Underground Hydrogen Storage

Underground hydrogen storage (UHS) is being evaluated as one of the possible technologies of energy storage on an industrial scale and over an extended period of time. The main geological reservoirs used for hydrogen storage include salt caverns, depleted oil and gas fields, and aquifers [1, 2]. These geological reservoirs have some major differences in regard to the storage process, geological properties, operational parameters, and technology development level. Salt caverns are among the most developed technologies for hydrogen storage, while porous media, including depleted reservoirs and aquifers, can offer a much larger storage capacity [1, 2].

One of the main features of UHS is its cyclical operation [3]. The process of hydrogen injection into the storage reservoir takes place during the injection cycle, while the withdrawal cycle implies the extraction of hydrogen from the storage reservoir [3]. The repeated injections and withdrawals could affect the pressure, the fluid distribution, and the hydrogen saturation in the storage reservoir [3].

2.2 Hydrogen Transport and Mixing

The mechanisms responsible for hydrogen transport through the geological formations include advection, dispersion, diffusion, dissolution, and hydrogen-rock-fluid interaction [1]. The influence and relative significance of these mechanisms depends on the characteristics of the storage formation and storage operation parameters. Hydrogen-rock-fluid interaction in porous-medium storage can lead to formation of a mixed zone between the hydrogen-rich plume and the surrounding fluids.

The development of this mixed zone is an important aspect when considering hydrogen recovery and withdrawal operations [1]. A large mixing zone means that a greater part of the hydrogen-containing region is influenced by the mixing process. This is why the development of the hydrogen plume and mixing zone gives additional information, which is not obtainable from the integrated hydrogen content.

The previous research suggests that hydrodynamics and biogeochemical processes are significant factors affecting hydrogen transport and storage in porous geological formations [1, 2]. Hydrogen transport during hydrogen injection and withdrawal is influenced by various factors, which include, but not limited to, formation heterogeneity, permeability, relative permeability, capillarity, diffusion, and dissolution [1, 3].

2.3 Effect of Operating Conditions

The operational mode is another significant factor affecting the performance of UHS [1]. The injection and withdrawal rates affect the flow of hydrogen through the storage medium and may affect the distribution of the hydrogen plume [1]. Hence, the operational factors may have an impact not only on the extent of plume expansion but also on the mixing of hydrogen and surrounding fluids.

Although numerical simulations and geological modeling are common methods for studying the large-scale behavior of UHS, laboratory experiments allow studying the spatiotemporal development of the hydrogen plume during repeated injections and withdrawals. Thus, repeated injection and withdrawal experiments can be used for studying the distribution and mixing of the hydrogen plume, accumulation and recovery of hydrogen.

2.4 Research Gap

The current literature base in relation to UHS offers detailed studies of geological storage methods, hydrogen transportation systems, and operation-related problems at the reservoir scale [1, 2]. It is also worth noting that a considerable amount of existing literature discusses geological-scale models, storage capacities, and the geochemistry and geomechanics of hydrogen within the underground formations [1, 2].

However, there seems to be relatively little consideration of the quantitative evaluation of changes in geometry of hydrogen plumes and properties of their mixing zones in relation to different injection/withdrawal cycles in controlled laboratory conditions. Particularly, the relationship between the injection rate, effective radius of the plume, thickness of the mixing zone, its area, integrated hydrogen content, and hydrogen recovery are of particular interest.

To bridge this knowledge gap, the current study analyzes three injection regimes—fast, moderate, and slow—based on the radial concentration profiles. The effective radius and properties of the mixing zone will be analyzed at the end of the injection and withdrawal phases of the respective cycles. Integrated hydrogen content and hydrogen recovery will be analyzed in order to compare the performance of the injection regimes.

3 Methodology

3.1 Experimental Overview

This study examines the development of hydrogen plumes over repeated injection–withdrawal cycles and evaluates the influence of injection rate on plume growth and mixing. Three experiments with different injection rates were investigated:

- Experiment 1: Fast injection
- Experiment 2: Intermediate injection
- Experiment 3: Slow injection

In each test, successive injections and withdrawals were performed similar to the cyclic operation related to hydrogen storage in the subsurface [3]. In order to analyze the radial profile of normalized hydrogen concentration during both injection and withdrawal processes, the three injection conditions were examined using the same approach to the analysis.

The experimental data were analyzed using MATLAB. For analyzing the radial spread of hydrogen plume, the effective radius was calculated, while the effective mixing layer thickness and effective area were also calculated for describing the mixing area surrounding the hydrogen plume. The integrated hydrogen content and hydrogen recovery were also determined.

3.2 Experimental Data and Cycle Definition

The experimental results were presented in the form of processed profiles of radial hydrogen concentration distributions, calculated from the experimental imaging data. Every processed image shows the distribution of normalized hydrogen concentration along the radius at a certain time.

The data were sorted based on separate injection and withdrawal cycles. One cycle includes one injection phase and one withdrawal phase. The number of complete cycles differs in different experiments. Experiments 1 and 3 include 26 injection–withdrawal cycles, while Experiment 2 includes 23 complete cycles. Thus, direct comparison of the cycles between experiments was limited only to the first 23 cycles, which is the common number for all the experiments. Extra cycles for Experiments 1 and 3 were taken into consideration when analyzing the long-term trend of these two experiments individually.

In order to analyze one cycle, the data were sorted into injection and withdrawal phases. Five typical profiles were chosen from each phase to analyze the hydrogen plume development:

1. Start of the stage
2. Approximately 25% of the stage
3. Approximately 50% of the stage
4. Approximately 75% of the stage
5. End of the stage

The representative processed-frame columns correspond to columns 1, 19, 38, 56, and 75 of each 75-frame injection or withdrawal segment. These profiles were used to calculate integrated hydrogen content, effective radius, mixing-zone thickness, and mixing-zone area.

3.3 Radial Concentration Analysis

The radial hydrogen concentration distribution was represented by the normalized concentration field $C(r, t)$, where r is the radial distance from the injection location and t is time.

The integrated hydrogen content was calculated from the radial concentration profile according to

$$H(t) = 2\pi \int C(r, t)\, r\, dr. \tag{1}$$

The integral was evaluated numerically using the trapezoidal integration method. Prior to integration, invalid or missing values were removed from both the radial coordinate and concentration arrays.

The same integration procedure was applied to the processed profiles used in the cycle-by-cycle analysis. Because the concentration field is normalized, the integrated quantity H has units of area (cm^2). It represents a radially integrated normalized concentration signal and therefore provides a relative measure of the hydrogen content within the observed plume rather than an absolute hydrogen mass.

3.4 Effective Radius

An effective radius was introduced to represent the spatial extent of the hydrogen plume using a single characteristic length scale. It was calculated from the integrated concentration as

$$R_{\text{eff}} = \sqrt{2 \int C(r)\, r\, dr}. \tag{2}$$

Since the hydrogen content defined in Eq. (1) is

$$H = 2\pi \int C(r)\, r\, dr, \tag{3}$$

the effective radius can also be related directly to the integrated hydrogen content by

$$R_{\text{eff}} = \sqrt{\frac{H}{\pi}}. \tag{4}$$

The effective radius was calculated independently for the five representative profiles within each injection and withdrawal stage. The end-of-injection and end-of-withdrawal values were then extracted for comparison between cycles and between experiments.

3.5 Mixing-Zone Thickness

The mixing zone was characterized using the region outside the effective radius. For a given radial concentration profile, the measured region satisfying

$$r \geq R_{\text{eff}} \tag{5}$$

was considered when evaluating the mixing characteristics.

A concentration-weighted mixing-zone thickness was calculated as

$$\Delta r = \frac{\displaystyle\int_{R_{\text{eff}}}^{r_{\max}} C(r)\, r\, (r - R_{\text{eff}})\, dr}{\displaystyle\int_{R_{\text{eff}}}^{r_{\max}} C(r)\, r\, dr}, \tag{6}$$

where $r_{\max}$ represents the maximum radial position available in the processed concentration profile.

This definition provides a concentration-weighted measure of the radial extent of the region outside the effective plume radius. The integrals were evaluated numerically using the trapezoidal integration method. The mixing-zone thickness was calculated for each representative profile during both injection and withdrawal.

3.6 Mixing-Zone Area

The mixing-zone area was calculated from the effective radius and mixing-zone thickness using the effective annular-area relationship

$$A_{\text{mix}} = 2\pi R_{\text{eff}} \Delta r. \tag{7}$$

This relationship defines a compact area measure for the mixing zone around the effective plume boundary. This relationship must be understood as an effective mixing zone area and not as the actual geometrical area of an annulus.

As a validation test, the mixing zone area values that were calculated were compared to the corresponding areas contained in the processed data. The maximum discrepancy between the calculated and the stored values was essentially zero in all three tests during injection and extraction.

3.7 Hydrogen Recovery

The hydrogen recovery metric was calculated by comparing the integrated hydrogen content at the end of withdrawal with that at the end of injection for each cycle:

$$\text{Recovery} = \frac{H_{\text{withdrawal}}}{H_{\text{injection}}} \times 100. \tag{8}$$

This indicator is defined as the proportion of integrated normalized hydrogen content retained in the analyzed plume after the withdrawal phase relative to the hydrogen content at the end of the injection phase. This is an indicator for hydrogen recovery in the analyzed region and should not be construed as the proportion of hydrogen actually extracted from the storage facility.

Recovery percentage was computed separately for each cycle, thereby determining the effect of cycling on hydrogen recovery with every new cycle.

3.8 Plume Expansion Rate

To quantify the characteristic rate of plume expansion during injection, the end-of-injection effective radius was plotted against elapsed experimental time.

The elapsed time corresponding to the end of injection for cycle i was calculated from the injection duration and cycle duration. A linear fit was then applied to the effective-radius data:

$$R_{\text{eff}}(t) = at + b, \tag{9}$$

where a represents the characteristic plume expansion rate,

$$\frac{dR_{\text{eff}}}{dt} = a. \tag{10}$$

The values for the expansion rates were then compared among the fast, intermediate, and slow injection cases. As the expansion rate is indicative of the growth rate with time for the effective radius, this quantity was evaluated independent of the effective radius itself.

3.9 Estimated Equivalent Injection Flow Rate

An estimated equivalent injection flow rate was obtained from the change in integrated hydrogen content associated with each injection stage.

The experimental thickness was taken as $h = 0.80$ cm. The equivalent volume associated with the integrated concentration was therefore estimated from

$$V_{\text{equiv}} = Hh, \tag{11}$$

where H is the integrated normalized hydrogen content and h is the assumed experimental thickness.

For the first injection cycle, the initial hydrogen content was taken as zero. The equivalent injection flow rate was therefore calculated as

$$Q_1 = \frac{H_{\text{injection},1}h}{\Delta t}. \tag{12}$$

For subsequent cycles, the equivalent injection flow rate was calculated from the difference between the hydrogen content at the end of the current injection stage and the hydrogen content at the end of the preceding withdrawal stage:

$$Q_i = \frac{\left(H_{\text{injection},i} - H_{\text{withdrawal},i-1}\right) h}{\Delta t}, \qquad i \geq 2. \tag{13}$$

Here, Δt is the injection duration, which was taken as 30 s. The resulting equivalent flow rates were converted from cm^3/s to m^3/s and compared between the three operating conditions.

Because H is based on a normalized concentration field rather than an absolute hydrogen mass measurement, the calculated Q values should be interpreted as estimated equivalent injection flow rates rather than direct measurements of the experimental volumetric flow rate.

3.10 Comparison Procedure

The three experiments were compared using the same analysis framework. The primary comparison parameters were:

- integrated hydrogen content at the end of injection;
- integrated hydrogen content at the end of withdrawal;
- effective radius;
- mixing-zone thickness;
- effective mixing-zone area;
- hydrogen recovery; and
- estimated equivalent injection flow rate.

Comparisons on a cycle-by-cycle basis have been done using the common range of the first 23 complete cycles. This allows for consistent comparison across all the three experiments as far as the fast, intermediate, and slow cases are considered with respect to the same number of complete injection-withdrawal cycles. Any extra cycles for Experiments 1 and 3 have been considered individually for analyzing their own trend but not as part of three-way comparison.

The analyses also took into account the development of the parameters with respect to cycle number and the relationship between plume size and mixing behavior. In particular, mixing zone thickness and mixing zone effective area have been analyzed as a function of effective radius.

For final value summaries, the last available complete cycle for each experiment has been presented separately as well. For these last available values, no three-way comparison has been considered since Experiment 2 has fewer complete cycles than Experiments 1 and 3. Common last complete cycle, which is Cycle 23, has been used for any direct comparison at a common cycle number.

3.11 Data Processing and Computational Tools

The entire data analysis was performed using MATLAB. The analysis scripts were developed to automatically analyze the available cycles and perform identical calculations for all three experiments.

The procedure included loading the data obtained from the experiment processing, separation of the injection and withdrawal cycles, selection of the characteristic profiles, rejection of invalid data, numerical integration of the radial concentration profiles, calculation of the effective radius and mixing zone, hydrogen recovery, equivalent injection flow rate, and plotting of the comparative graphs and generation of the tables.

The processed data for Experiments 1-3 were exported as MATLAB data file and further loaded by the comparison script. The comparison script calculated the parameters at the end of the injection and withdrawal cycles and plotted the comparative graphs and tables.

4 Results

4.1 Overview of Experimental Results

A total of three experiments were taken into consideration to examine the effects of the hydrogen injection rate on plume dynamics, mixing, and hydrogen recovery. Experiment 1 was for the fast injection rate, Experiment 2 for the intermediate injection rate, and Experiment 3 for the slow injection rate.

There were 27, 24, and 27 injection stages in each experiment. Because the cycle comprises injection and withdrawal stages, there were 26, 23, and 26 complete injection-withdrawal cycles in fast, intermediate, and slow injection experiments, respectively. As a result, comparisons between both injection and withdrawal stages could be made only for the first 23 complete cycles since it is the common range for all three experiments.

Variables compared were: effective radius, integrated normalized hydrogen content, mixing zone thickness, effective mixing zone area, hydrogen recovery, plume expansion rate, and estimated equivalent injection flow rate.

4.2 Effective Radius

The effective radius, R_{eff}, was used to characterise the radial extent of the hydrogen plume. Figure 1 presents the effective radius at the end of injection for the three experiments.

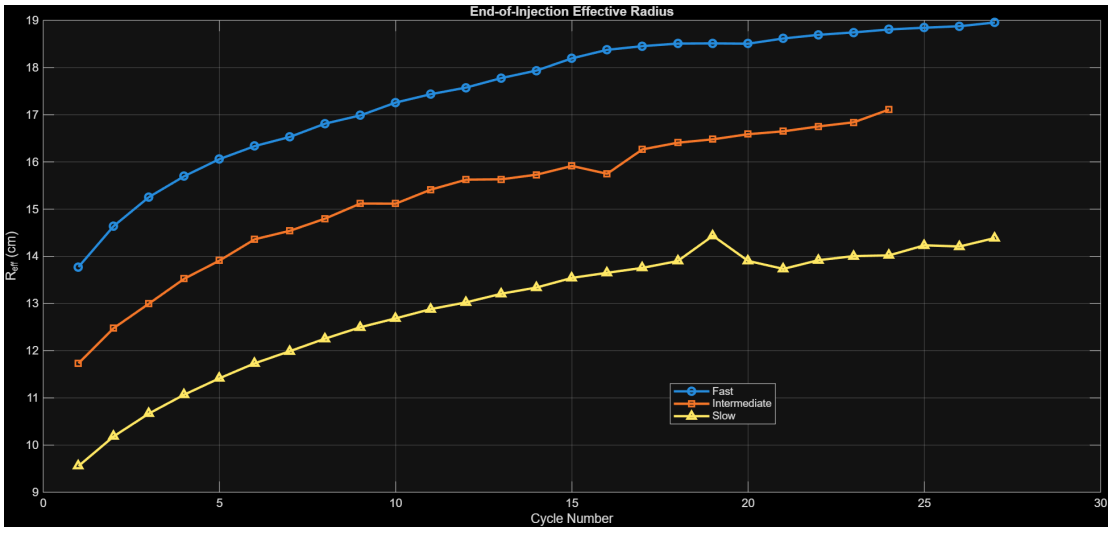


Figure 1 Effective radius at the end of injection for the fast, intermediate, and slow injection experiments.

A noticeable difference can be seen among the three injection tests. As expected, the fast test usually has a greater effective radius than the intermediate and slow tests. The rate of increase of the effective radius was very high at the start of the test period and became much slower afterwards.

In the case of the final complete cycle from each test, the effective radii after the process of injection were 18.876 cm, 16.841 cm, and 14.208 cm in the fast, intermediate, and slow tests, respectively. In this case, the three Cycles 26, 23, and 26 were selected; thus, the comparison cannot be made on the basis of a common cycle.

In the case of the common final complete cycle, which is Cycle 23, the respective effective radii were 18.745 cm, 16.841 cm, and 14.004 cm in the fast, intermediate, and slow tests, respectively. Hence, the order of plume size at this common point of comparison was

$$R_{\text{eff,Fast}} > R_{\text{eff,Intermediate}} > R_{\text{eff,Slow}}. \tag{14}$$

Figure 2 shows the corresponding effective radius at the end of withdrawal.

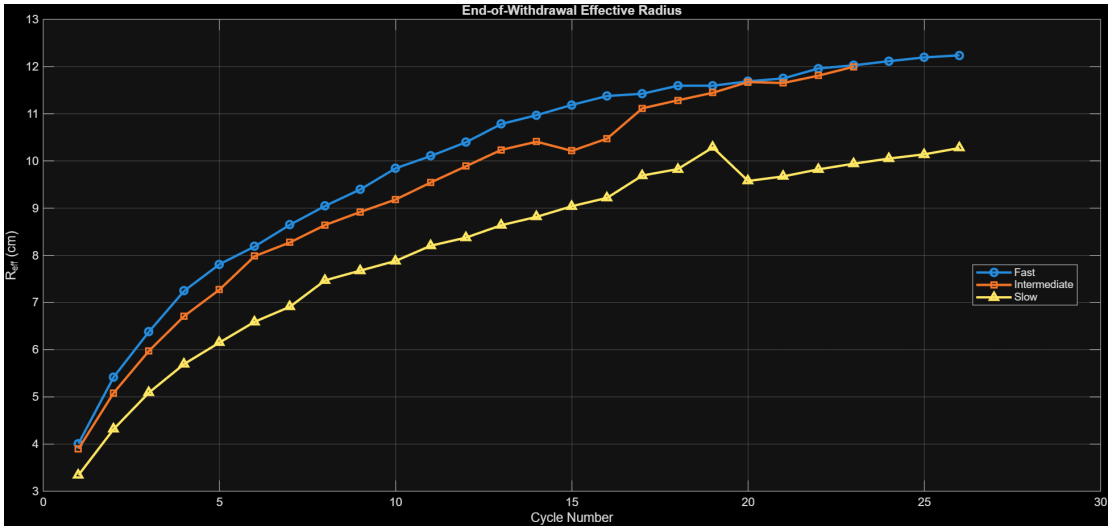


Figure 2 Effective radius at the end of withdrawal for the three injection conditions.

The effective radius decreased substantially during withdrawal, reflecting hydrogen removal and redistribution within the experimental domain. However, the fast experiment generally maintained the largest effective radius, whereas the slow experiment maintained the smallest.

At the final complete cycle available for each experiment, the end-of-withdrawal effective radii were 12.238 cm, 11.997 cm, and 10.274 cm for the fast, intermediate, and slow experiments, respectively.

4.3 Integrated Normalized Hydrogen Content

Figure 3 shows the integrated normalized hydrogen content at the end of injection and end of withdrawal.

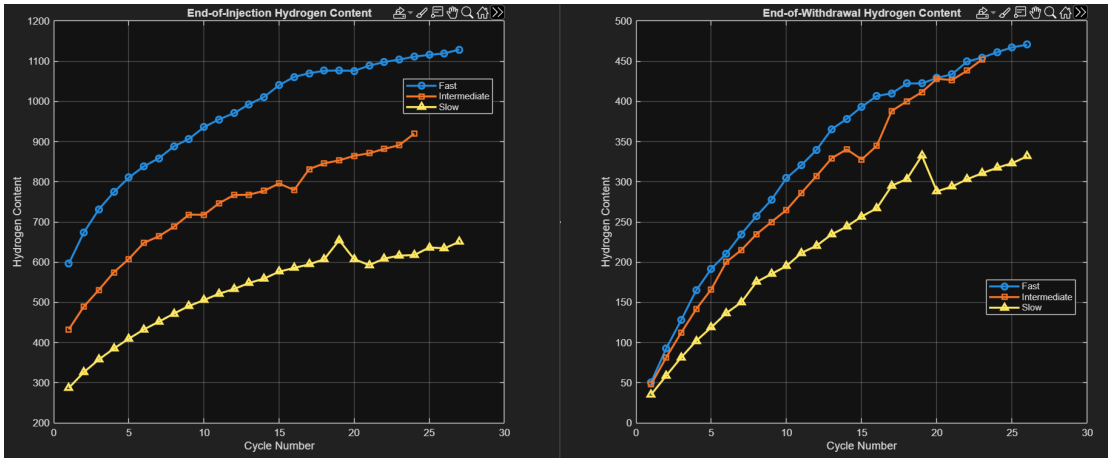


Figure 3 Integrated normalized hydrogen content at the end of injection and withdrawal for the three injection conditions.

The integrated normalized hydrogen content after injection showed an increasing trend with

respect to the number of cycles in all three experiments. The fast experiment had a greater amount of integrated hydrogen content compared to the intermediate and slow experiments.

For the last complete cycle available in each experiment, the integrated hydrogen content after injection was 1119.4, 890.99, and 634.22, respectively, for the fast, intermediate, and slow experiments. The corresponding value after withdrawal was 470.52, 452.17, and 331.64, respectively.

An increase in the integrated hydrogen content after each cycle suggests that there is a continuous buildup of the normalized hydrogen content within the scope of the experimental domain. The faster equivalent injection flow rate observed in the fast experiment explains its higher integrated hydrogen content.

The normalized concentration field explains why the results have to be considered in terms of integration rather than actual hydrogen content.

4.4 Hydrogen Recovery

Hydrogen recovery represents the fraction of the integrated normalized hydrogen content that remains after the withdrawal stage relative to the amount present at the end of injection. The recovery trends are presented in Figure 4.

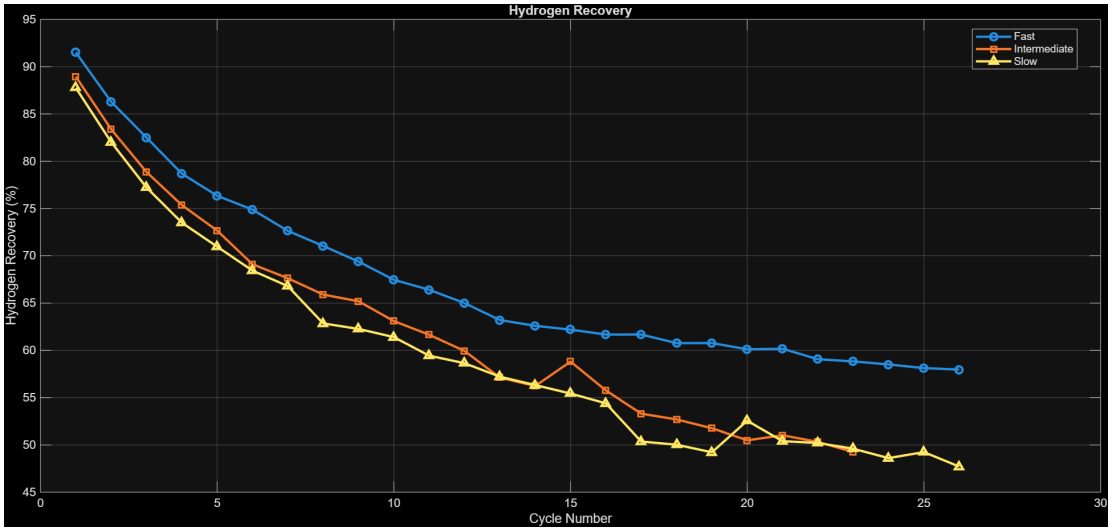


Figure 4 Hydrogen recovery as a function of cycle number for the three injection conditions.

The decrease in hydrogen recovery in the first cycles is apparent in all three cases. The fast case starts with a recovery level of approximately 92%, whereas the intermediate and slow cases start at 89% and 88%, respectively.

Recovery decreases further as the number of cycles increases. The fast case keeps higher than the other two until most of the experimental duration. At the last full cycle that could be obtained from the experiments, the recovery was 57.97%, 49.25%, and 47.71% for the fast, intermediate, and slow cases, respectively.

At the last full cycle in common, which is Cycle 23, the recovery values were approximately 58.83%, 49.25%, and 49.60% for the fast, intermediate, and slow cases, respectively. Hence, the fast case had the highest retained fraction in common, while the other two cases were almost equal.

The recovery parameter refers to the percentage of the integrated normalized hydrogen content that remained in the selected analyzed region after the withdrawal. Therefore, it does not refer to the fraction of hydrogen recovered from the experiment.

4.5 Mixing-Zone Thickness

The mixing-zone thickness, Δr, characterises the radial thickness of the transition region surrounding the effective hydrogen plume.

Figure 5 presents the mixing-zone thickness at the end of injection.

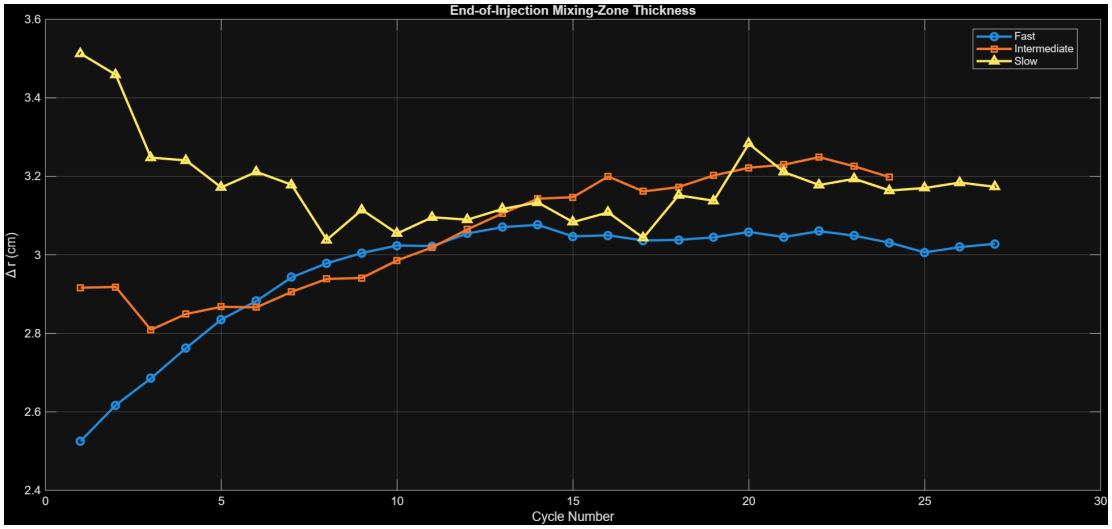


Figure 5 End-of-injection mixing-zone thickness for the three injection conditions.

The thickness of the mixing zone varied during the course of the injection process and showed different trends for the three experiments conducted. In the fast experiment, the mixing zone thickness started out relatively small and then progressively increased to eventually reach an approximate equilibrium range of 3.0–3.1 cm.

In the intermediate experiment, it increased from approximately 2.8 cm to values of 3.2–3.25 cm. In the slow experiment, it started out as the largest of the three at approximately 3.5 cm and then decreased before oscillating around values of approximately 3.1–3.2 cm.

For the end-of-injection point in each experiment, the thicknesses were found to be 3.020 cm, 3.226 cm, and 3.184 cm for the fast, intermediate, and slow experiments, respectively.

This indicates that the injection rate affects the radial size of the plume more significantly than the thickness of the mixing zone.

The corresponding end-of-withdrawal results are shown in Figure 6.

After the withdrawal period, a relatively large mixing zone was observed compared to after the injection period. After the completion of the fast experiment, it converged at approximately 4.7–4.9 cm; however, after the completion of the intermediate experiment, it converged at about 4.0–4.2 cm.

The slow experiment had the greatest thickness of the initial mixing zone at approximately 8.2 cm, after which it sharply decreased and oscillated between 4.0 cm and 4.5 cm.

At the last complete cycle of each experiment, the thicknesses of the end-of-withdrawal mixing zones were 4.669 cm, 4.070 cm, and 3.933 cm

4.6 Mixing-Zone Area

The effective mixing-zone area was calculated from the effective radius and mixing-zone thickness according to

$$A_{\text{mix}} = 2\pi R_{\text{eff}} \Delta r. \tag{15}$$

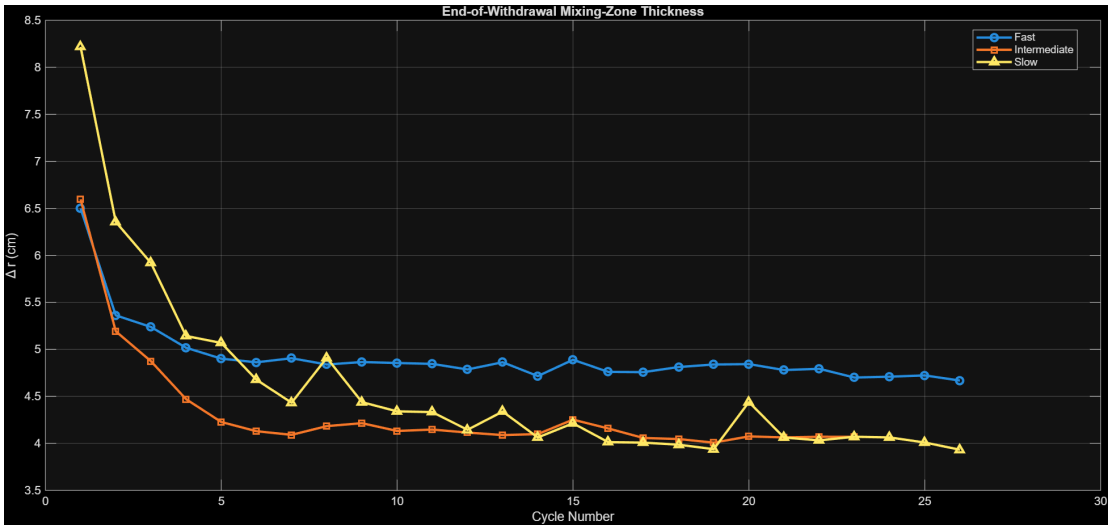


Figure 6 End-of-withdrawal mixing-zone thickness for the three injection conditions.

This quantity is treated as an effective mixing-zone area metric rather than the exact geometrical area of an annulus.

The end-of-injection mixing-zone areas are shown in Figure 7.

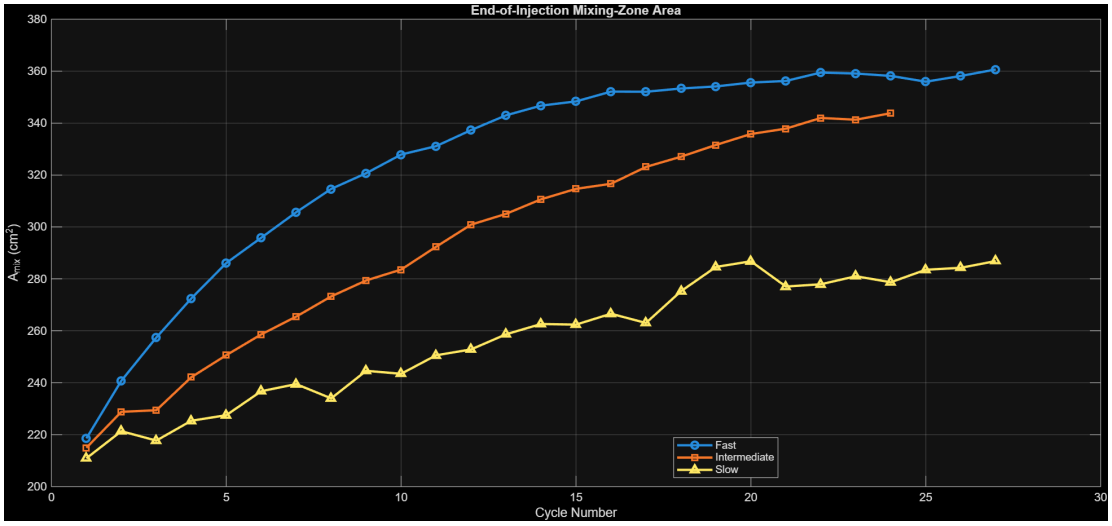


Figure 7 End-of-injection effective mixing-zone area for the three injection conditions.

The effective mixing-zone area increased with cycle number for all three experiments. The fast experiment exhibited the largest area throughout most of the experiment, reaching approximately 358 cm^2 at its final available complete cycle.

The intermediate experiment reached approximately 341 cm^2, while the slow experiment reached approximately 284 cm^2.

The ordering of the effective mixing-zone areas therefore followed the ordering of the effective radius:

$$A_{\mathrm{mix,Fast}} > A_{\mathrm{mix,Intermediate}} > A_{\mathrm{mix,Slow}}. \tag{16}$$

This result indicates that the larger plume produced under faster injection conditions was associated with a larger overall effective region occupied by the mixing-zone metric.

Figure 8 shows the effective mixing-zone area after withdrawal.

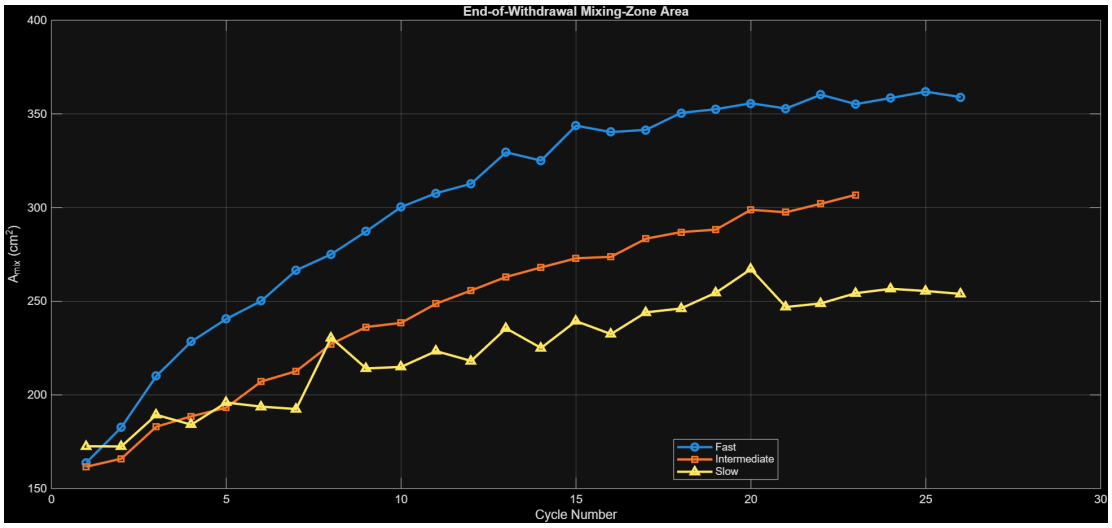


Figure 8 End-of-withdrawal effective mixing-zone area for the three injection conditions.

At the final complete cycle available for each experiment, the end-of-withdrawal effective mixing-zone areas were approximately 358.98 cm^2, 306.81 cm^2, and 253.90 cm^2 for the fast, intermediate, and slow experiments, respectively.

The fast experiment maintained a mixing-zone area after withdrawal that was close to its end-of-injection value. This occurs because the decrease in effective radius during withdrawal was accompanied by an increase in mixing-zone thickness.

4.7 Relationship Between Mixing-Zone Thickness and Effective Radius

The relationship between mixing-zone thickness and effective radius provides information about how the mixing zone develops as the plume expands or contracts.

Figure 9 presents this relationship during injection and withdrawal.

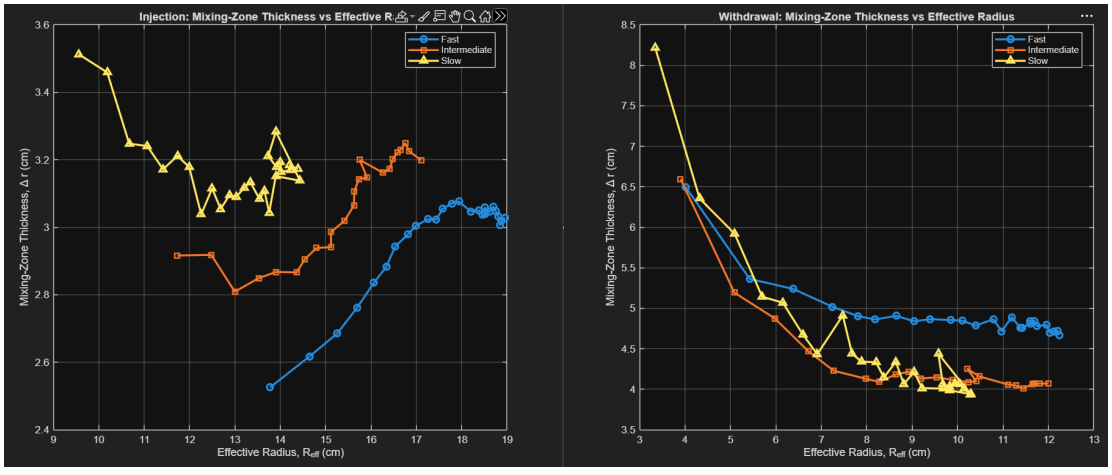


Figure 9 Mixing-zone thickness as a function of effective radius during injection and withdrawal.

In the case of injection, the thickness of the mixing zone fell within a relatively narrow range regardless of significant differences in the effective radius value. The fast experiment covered approximately 2.53–3.08 cm, while the intermediate and slow experiments covered approximately 2.81–3.25 cm and 3.04–3.51 cm, respectively.

It shows that an increase in the injection rate mostly influences the size of the plume, not the thickness of the mixing zone.

For the withdrawal process, different characteristics can be traced. The mixing-zone thickness was larger for smaller effective radius values and became smaller as the effective radius increased. Such tendency was more distinct for the slow experiment, where the thickness of the mixing zone changed from approximately 8.22 cm to 4 cm.

4.8 Relationship Between Mixing-Zone Area and Effective Radius

Figure 10 shows the effective mixing-zone area as a function of effective radius.

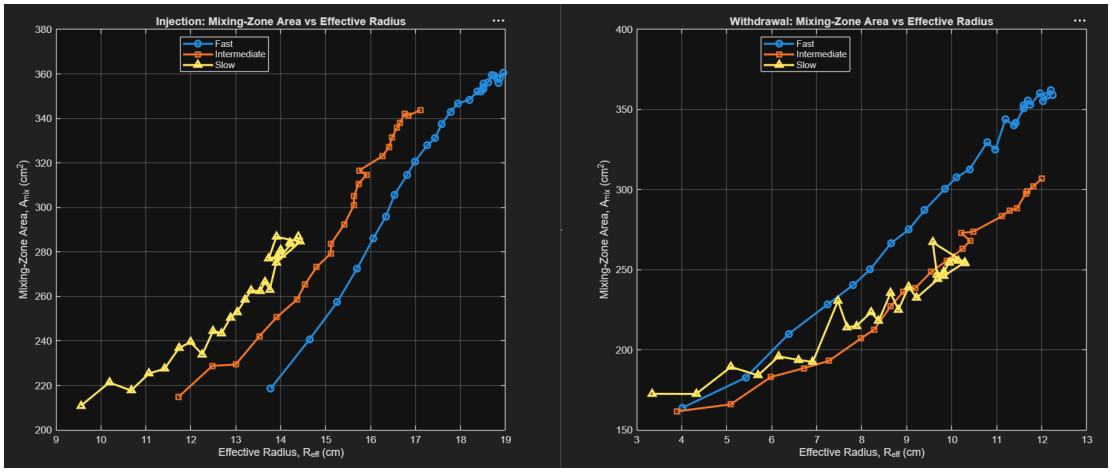


Figure 10 Effective mixing-zone area as a function of effective radius during injection and withdrawal.

The effective mixing-zone area increased systematically with effective radius during injection for the three experiments. The fast experiment attained the greatest effective radius and therefore the greatest effective mixing-zone area, while the slow experiment remained lower in both measures.

The withdrawal results showed a similar overall positive relationship between effective radius and effective mixing-zone area, although greater cycle-to-cycle variability was observed. This relationship is expected from the definition of the area metric:

$$A_{\text{mix}} = 2\pi R_{\text{eff}} \Delta r. \tag{17}$$

The numerical consistency of this relationship was verified using the experimental data. The maximum difference between the calculated and stored mixing-zone areas was 0.000000 cm^2 for all three experiments during both injection and withdrawal.

4.9 Plume Expansion Rate

The effective radius at the end of injection was plotted against elapsed injection time to estimate the characteristic rate of plume expansion.

A linear relationship of the form

$$R_{\text{eff}}(t) = at + b \tag{18}$$

was fitted independently to each experiment, where a represents the characteristic plume expansion rate.

Figure 11 shows the measured effective radius and the corresponding linear fits.

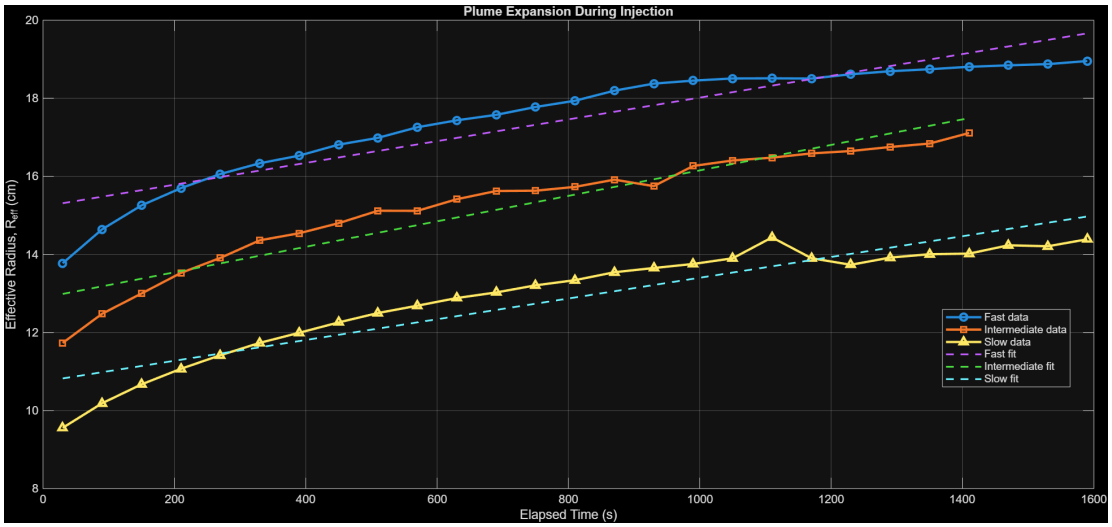


Figure 11 Effective radius as a function of elapsed time during injection and corresponding linear fits.

The fitted expansion rates were

$$\left(\frac{dR_{\text{eff}}}{dt}\right)_{\text{Fast}} = 0.002790 \text{ cm/s}, \tag{19}$$

$$\left(\frac{dR_{\text{eff}}}{dt}\right)_{\text{Intermediate}} = 0.003265 \text{ cm/s}, \tag{20}$$

and

$$\left(\frac{dR_{\text{eff}}}{dt}\right)_{\text{Slow}} = 0.002660 \text{ cm/s}. \tag{21}$$

Therefore, the intermediate experiment showed the largest fitted temporal expansion rate even though the estimated equivalent injection flow rate was smaller compared to that of the fast experiment. The above observations suggest that the fitted temporal expansion rate does not show a direct correlation with the estimated equivalent injection flow rate.

The above observations might be related to the developing concentration profile and the accumulated effects on the distribution and mixing of hydrogen during successive cycles. As such, the effective radius at a certain cycle and the fitted temporal expansion rate capture different characteristics of the plume development process.

4.10 Estimated Equivalent Injection Flow Rate

The estimated equivalent injection flow rate was calculated from the change in integrated normalized hydrogen content associated with each 30 s injection period. The assumed experimental thickness was 0.80 cm.

For the first injection cycle,

$$Q_1 = \frac{H_{\text{injection},1}\, h}{\Delta t}. \tag{22}$$

For subsequent cycles,

$$Q_i = \frac{\left(H_{\text{injection},i} - H_{\text{withdrawal},i-1}\right) h}{\Delta t}, \qquad i \geq 2. \tag{23}$$

The estimated equivalent flow-rate results are shown in Figure 12.

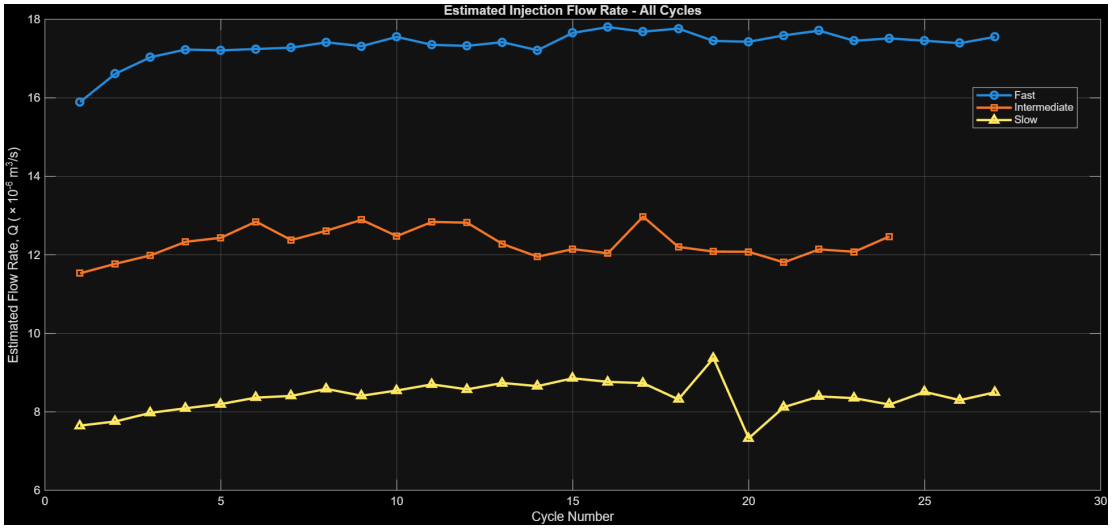


Figure 12 Estimated equivalent injection flow rate for all injection cycles.

The mean estimated equivalent flow rates over all available injection stages were

$$\overline{Q}_{\text{Fast}} = 1.7354 \times 10^{-5}\ \text{m}^3/\text{s}, \tag{24}$$

$$\overline{Q}_{\text{Intermediate}} = 1.2299 \times 10^{-5}\ \text{m}^3/\text{s}, \tag{25}$$

and

$$\overline{Q}_{\text{Slow}} = 8.3834 \times 10^{-6}\ \text{m}^3/\text{s}. \tag{26}$$

Thus, the estimated equivalent injection flow rates follow the intended experimental ordering:

$$Q_{\text{Fast}} > Q_{\text{Intermediate}} > Q_{\text{Slow}}. \tag{27}$$

The fast experiment had an estimated mean equivalent flow rate approximately 41% higher than the intermediate experiment and approximately 107% higher than the slow experiment. Despite these differences in injection rate, the fitted plume expansion rates were relatively similar, indicating that the relationship between injection rate and temporal plume expansion was not directly proportional.

The estimated equivalent flow rates remained relatively stable over most cycles. The slow experiment exhibited a larger fluctuation around Cycles 19–20, whereas the fast and intermediate experiments remained comparatively stable.

Because the integrated hydrogen content is based on normalized concentration data, these values should be interpreted as estimated equivalent flow rates rather than direct measurements of the experimental volumetric flow rate.

4.11 Overall Comparison of Injection Conditions

Table 1 summarises the principal final available results from the three experiments.

The final available values reveal that the fast injection condition gave rise to the biggest effective plume radius, the maximum value of the integrated normalized hydrogen content, and

Table 1 Summary of the final available values for the three injection conditions

Parameter	Fast	Intermediate	Slow
Last complete cycle	26	23	26
Mean flow rate (10^{-5} m^3/s)	1.7354	1.2299	0.8383
R_{eff} at injection (cm)	18.876	16.841	14.208
Δr at injection (cm)	3.020	3.226	3.184
A_{mix} at injection (cm^2)	358.14	341.30	284.26
R_{eff} at withdrawal (cm)	12.238	11.997	10.274
Δr at withdrawal (cm)	4.669	4.070	3.933
A_{mix} at withdrawal (cm^2)	358.98	306.81	253.90
Hydrogen recovery (%)	57.97	49.25	47.71

the biggest effective mixing-zone area. The slow injection condition led to the minimum values of these plume characteristics.

However, the mixing-zone thickness was not related to the order of the estimated equivalent injection flow rate. At the end of the injection process, the fast experiment yielded the lowest final available mixing-zone thickness, whereas the intermediate and slow experiments revealed higher values. Therefore, it may be concluded that injection rate has a greater effect on plume size and integrated hydrogen content than on mixing-zone thickness.

Overall, the results have shown that injection rate is an important factor in determining plume size and integrated normalized hydrogen content, but its impact on mixing-zone thickness and fitted temporal plume expansion rate is less significant.

In order to compare the results of three experiments directly in the same cycle number, Cycle 23 should be used as the last cycle of all experiments.

5 Discussion

5.1 Effect of Injection Rate on Plume Development

The comparison of the three experiments demonstrates a clear influence of injection rate on the overall development of the hydrogen plume. The estimated mean equivalent injection flow rates were 1.7354×10^{-5}, 1.2299×10^{-5}, and 8.3834×10^{-6} m^3/s for the fast, intermediate, and slow experiments, respectively. Thus, the three experimental conditions provide a clear ordering of the estimated equivalent injection rate from fast to slow.

A similar ordering was observed for the effective radius and integrated normalized hydrogen content. At the final complete cycle available for each experiment, the effective radii at the end of injection were 18.876 cm, 16.841 cm, and 14.208 cm for the fast, intermediate, and slow experiments, respectively. The corresponding integrated normalized hydrogen contents were 1119.4, 890.99, and 634.22.

However, these final available values correspond to different cycle numbers: Cycle 26 for the fast and slow experiments and Cycle 23 for the intermediate experiment. Therefore, they should not be interpreted as a direct same-cycle comparison. At the common final complete cycle, Cycle 23, the effective radii were 18.745 cm, 16.841 cm, and 14.004 cm for the fast, intermediate, and slow experiments, respectively. The corresponding integrated normalized hydrogen contents were 1103.92, 890.99, and 616.14.

The consistent ordering indicates that higher injection rates are associated with larger plume radii and higher integrated normalized hydrogen content within the observed experimental

domain. This is consistent with previous experimental findings that higher injection rates can promote greater hydrogen accumulation and larger plume development during cyclic injection tests. Since the injection duration was the same for the three experiments, a higher injection rate allows a greater quantity of hydrogen to be introduced during each injection stage.

Therefore, the findings indicate that injection rate plays an important role in determining the overall radial extent of the hydrogen plume and the integrated hydrogen content. Nevertheless, the influence of injection rate is not identical for all measured parameters, as discussed in the following sections.

5.2 Plume Size and Hydrogen Accumulation

The relationship between integrated normalized hydrogen content and effective radius is one of the important findings of the experiments. The fast experiment generally exhibited the highest values of both integrated hydrogen content and effective radius, whereas the slow experiment generally exhibited the lowest values.

The difference becomes more evident as the number of cycles increases. Repeated injection and withdrawal can alter the spatial distribution of hydrogen and may contribute to redistribution and trapping within the experimental domain [3]. The higher estimated equivalent injection rate in the fast experiment therefore resulted in greater accumulation of the normalized hydrogen signal and a larger hydrogen-rich region over successive cycles.

The effective mixing-zone area followed a similar overall trend. At the final available complete cycle, the end-of-injection effective mixing-zone areas were approximately 358.14 cm^2, 341.30 cm^2, and 284.26 cm^2 for the fast, intermediate, and slow experiments, respectively.

This behaviour is consistent with the effective-area relationship

$$A_{\mathrm{mix}} = 2\pi R_{\mathrm{eff}} \Delta r. \tag{28}$$

Since the fast experiment developed a substantially larger effective radius, it produced a larger effective mixing-zone area even though its mixing-zone thickness was not the largest. This distinction is important because it demonstrates that the effective mixing-zone area depends on both the radial extent of the plume and the thickness of the surrounding mixing region.

5.3 Behaviour of the Mixing Zone

The mixing-zone thickness showed a different behaviour from the effective radius. At the final available complete cycle, the end-of-injection mixing-zone thicknesses were approximately 3.02 cm, 3.23 cm, and 3.18 cm for the fast, intermediate, and slow experiments, respectively.

Thus, the experiment with the largest plume radius did not produce the largest mixing-zone thickness. Instead, the fast experiment generally exhibited the smallest mixing-zone thickness during injection.

This indicates that increasing the injection rate primarily affected the radial expansion of the hydrogen-rich plume rather than producing a proportional increase in the thickness of the transition region.

The difference became more apparent during withdrawal. The mixing-zone thickness increased substantially relative to the end-of-injection condition. At the final available complete cycle, the thicknesses were approximately 4.67 cm, 4.07 cm, and 3.93 cm for the fast, intermediate, and slow experiments, respectively.

The increase in mixing-zone thickness during withdrawal indicates that withdrawal altered the spatial distribution of hydrogen and produced a broader transition region around the effective

plume boundary. The simultaneous reduction in effective radius demonstrates that withdrawal did not simply produce a geometrically scaled-down version of the injection-stage plume.

This behaviour is qualitatively consistent with the complex transport and hysteresis effects that can occur during multiphase flow in porous media [3]. However, the present experiments do not independently identify hysteresis as the specific mechanism responsible for the observed changes. The results therefore indicate a change in plume distribution during withdrawal rather than directly proving the contribution of any individual transport mechanism.

5.4 Hydrogen Recovery During Repeated Cycling

Hydrogen recovery decreased progressively with cycle number for all three experiments. The fast experiment began with a recovery of approximately 92%, while the intermediate and slow experiments began at approximately 89% and 88%, respectively.

At the final available complete cycle, the recovery values decreased to approximately 58.0% for the fast experiment, 49.3% for the intermediate experiment, and 47.7% for the slow experiment.

At the common final complete cycle, Cycle 23, the corresponding recovery values were approximately 58.83%, 49.25%, and 49.60% for the fast, intermediate, and slow experiments, respectively. Therefore, the fast experiment exhibited the highest retained fraction at the common comparison point, while the intermediate and slow experiments showed relatively similar retention.

The progressive decrease in recovery indicates that an increasing fraction of the integrated normalized hydrogen content was not located within the effective hydrogen-rich region at the end of withdrawal. This may be associated with redistribution of hydrogen into the surrounding mixing region and other transport processes occurring during repeated cycling [3].

The fast experiment generally maintained the highest recovery during most of the experimental period. This behaviour is consistent with its larger hydrogen-rich plume and higher integrated normalized hydrogen content. However, the results do not indicate that injection rate alone controls recovery, because recovery also depends on the spatial distribution and evolution of hydrogen during the injection and withdrawal stages.

5.5 Plume Expansion Rate

Although the fast experiment produced the largest plume and the highest estimated equivalent injection flow rate, it did not produce the largest fitted temporal plume expansion rate.

The fitted values of dR_{eff}/dt were 0.002790 cm/s, 0.003265 cm/s, and 0.002660 cm/s for the fast, intermediate, and slow experiments, respectively. The intermediate experiment therefore exhibited the highest fitted radial expansion rate.

This result demonstrates that the fitted temporal growth of the effective radius was not directly proportional to the estimated equivalent injection flow rate.

The difference may be related to the evolving radial concentration distribution, development of the mixing region, and cumulative changes resulting from repeated injection and withdrawal. Therefore, the amount of hydrogen introduced into the system is not the only factor determining the temporal growth of the effective radius.

The result also demonstrates that plume size and plume growth rate represent different characteristics of plume development. The fast experiment ultimately produced the largest effective radius, but its fitted temporal expansion rate was lower than that of the intermediate experiment. This suggests that the fast experiment accumulated a larger integrated hydrogen content and developed a larger plume over the experimental period without necessarily exhibiting the highest fitted rate of radial expansion.

5.6 Injection and Withdrawal Behaviour

The comparison between injection and withdrawal highlights the different behaviour of the plume during the two stages of the cycle.

The effective radius and integrated normalized hydrogen content generally increased with cycle number during the injection process. This indicates that the plume became progressively larger and that the integrated hydrogen signal increased over repeated injection stages.

During withdrawal, the effective radius decreased, whereas the mixing-zone thickness generally increased relative to the injection condition. This behaviour demonstrates that withdrawal changed the spatial distribution of hydrogen rather than simply reversing the injection process.

The effective mixing-zone area remained substantial after withdrawal. For example, in the fast experiment, the final available end-of-withdrawal effective mixing-zone area was approximately 358.98 cm^2, compared with 358.14 cm^2 at the end of injection. This occurred despite a reduction in effective radius from 18.88 cm to 12.24 cm because the mixing-zone thickness increased from 3.02 cm to 4.67 cm.

This example demonstrates the importance of considering both effective radius and mixing-zone thickness when characterising the spatial distribution of hydrogen. Effective radius alone does not fully describe the extent of the surrounding mixed region.

5.7 Implications of the Experimental Comparison

The results indicate that injection rate is an important parameter affecting the integrated normalized hydrogen content and radial extent of the plume. The fast injection condition was associated with the largest effective radius, highest integrated normalized hydrogen content, and largest effective mixing-zone area.

However, the results also demonstrate that plume behaviour cannot be explained by injection rate alone. The mixing-zone thickness did not follow the same ordering as the estimated equivalent injection flow rate, and the fitted temporal plume expansion rate was highest for the intermediate experiment rather than the fast experiment.

These findings indicate that increasing the injection rate can produce a larger hydrogen-rich region without a proportional increase in mixing-zone thickness or fitted temporal plume expansion rate.

Overall, the experimental data suggest that plume development results from the combined influence of injection rate, repeated cycling, and evolution of the surrounding mixing region. This interpretation is consistent with the general understanding that hydrogen migration in porous media can be influenced by multiphase flow, trapping, dispersion, and fluid–rock interactions [1, 3]. The present experiments provide an experimental perspective on these effects by directly relating the evolution of plume geometry and mixing-zone characteristics to changes in integrated normalized hydrogen content and hydrogen recovery.

6 Limitations and Future Work

6.1 Limitations

Several limitations should be considered when interpreting the results of this study.

First, the injection flow rates were not measured directly using a flow meter. Instead, an estimated equivalent injection flow rate was calculated from the integrated normalized hydrogen content, an assumed experimental thickness of 0.80 cm, and the injection duration of 30 s. Therefore, the resulting flow-rate values should be interpreted as estimated equivalent flow

rates rather than direct measurements of the experimental volumetric flow rate. The values are nevertheless useful for comparing the relative injection conditions between the three experiments.

Second, the three experiments did not contain the same number of complete injection–withdrawal cycles. Experiments 1 and 3 contained 26 complete cycles, whereas Experiment 2 contained 23 complete cycles. Consequently, direct three-way comparisons were restricted to the first 23 complete cycles. The additional cycles available for Experiments 1 and 3 were retained for examining their individual long-term trends but were not used for direct same-cycle comparisons.

Third, the integrated hydrogen content used in this study was derived from normalized concentration profiles rather than from an absolute concentration calibration. Consequently, the integrated quantity H represents a radially integrated normalized concentration signal and should not be interpreted as an absolute hydrogen mass. Similarly, the hydrogen recovery metric represents the fraction of this integrated normalized signal remaining after withdrawal rather than the fraction of hydrogen physically recovered from the experimental system.

Fourth, the effective radius and mixing-zone thickness were determined from image-based concentration profiles. Since the boundary between the hydrogen-rich region and the surrounding medium may be gradual, uncertainty is associated with the identification and characterization of the plume and mixing region. These uncertainties may affect the calculated effective radius, mixing-zone thickness, and effective mixing-zone area.

The effective-radius approach also simplifies the actual plume geometry into a single characteristic length scale. The experimental plume may not be perfectly circular or radially symmetric, particularly during transient injection and withdrawal stages. Therefore, the effective radius provides a convenient quantitative measure of plume extent but does not capture all spatial variations in the hydrogen concentration field.

Finally, cycle-to-cycle fluctuations were observed in several parameters, particularly in the slow injection experiment. These fluctuations may arise from experimental variability, image-processing uncertainty, or changes in the spatial distribution and geometry of the plume between successive cycles. Without repeated experiments under identical conditions, it is difficult to separate systematic effects from random experimental variability.

6.2 Future Work

Several extensions could improve the analysis and provide a more complete understanding of the influence of injection rate on hydrogen plume behaviour.

Direct measurement of the injection flow rate using a calibrated flow meter would be an important first step. Such measurements would allow the relationship between the actual injection flow rate and plume development to be established without relying on the assumed experimental thickness used in the current equivalent flow-rate estimation.

Additional experiments at intermediate injection rates could also be performed to provide a wider range of operating conditions. Such experiments would help determine whether the relationships between injection rate, integrated hydrogen content, effective radius, mixing-zone thickness, and effective mixing-zone area are approximately linear or exhibit nonlinear behaviour.

Repeating each injection condition under identical experimental conditions would provide a measure of experimental repeatability and associated uncertainty. Replicate experiments would help distinguish systematic trends caused by differences in injection rate from random experimental variations and image-processing uncertainty.

Future image analysis could also extend beyond the effective-radius approach by quantifying the complete two-dimensional spatial distribution of the hydrogen-enriched region. Such an approach could capture plume asymmetry and local variations that are not represented by a

single effective radius.

A further improvement would be to develop an experimentally calibrated relationship between image intensity and absolute hydrogen concentration. This would enable the integrated concentration signal to be converted into an estimate of absolute hydrogen quantity, provided that the necessary calibration and experimental assumptions are established.

Finally, a physical transport model could be developed to examine the relationship between injection rate, plume growth, mixing-zone formation, and hydrogen recovery [1]. Such a model could help explain why the intermediate experiment exhibited the highest fitted radial plume-growth rate despite having a lower estimated equivalent injection flow rate than the fast experiment. The model could also be used to investigate the relative contributions of transport, dispersion, mixing, and repeated injection–withdrawal cycling to the observed plume behaviour.

7 Conclusion

This study tried to establish the effects of hydrogen injection rates on plume formation, hydrogen deposition, mixing process, and hydrogen recovery over several cycles of injection and removal. There were three cases of experiments conducted in relation to hydrogen injection rates: fast, intermediate, and slow injection rates. The basis of the analysis is the development of effective radius, mixing zone thickness, mixing zone area, hydrogen concentration, and hydrogen recovery.

The results clearly demonstrate the effect of hydrogen injection rates on the development of plume. For example, the fast injection case resulted in the largest effective radius at the end of the injection of about 18.9 centimeters, as opposed to 16.8 centimeters and 14.2 centimeters for the intermediate and slow injections, respectively.

The characteristics of the mixing zones for the three methods of injection varied as well. Towards the end of the injection process, the thickness of the mixing zone was relatively uniform at around 3 cm in the three methods, although the slow method had a slightly larger mixing zone than the others. The area of the mixing zone also increased throughout the testing process due to the increasing plume size, with the fast test having the largest mixing zone area, followed by the intermediate and slow tests. The area of the mixing zone also conformed to the following relationship

$$A_{\text{mix}} = 2\pi R_{\text{eff}} \Delta r.$$

During withdrawal, the effective radius and hydrogen content decreased as hydrogen was removed from the system. Nevertheless, the fast experiment retained the largest hydrogen content and effective radius throughout most of the observed cycles. At the final complete cycle of each experiment, the hydrogen recovery was approximately 58.0% for the fast experiment, 49.3% for the intermediate experiment, and 47.7% for the slow experiment. These results indicate that the higher injection-rate condition produced not only a larger plume during injection but also a greater amount of hydrogen remaining in the system after withdrawal.

The estimated equivalent injection flow rates followed the expected ordering of the three experimental conditions. The mean estimated flow rates were approximately 1.74×10^{-5} m^3/s for the fast experiment, 1.23×10^{-5} m^3/s for the intermediate experiment, and 8.38×10^{-6} m^3/s for the slow experiment. The estimated plume growth rates were approximately 0.00279, 0.00327, and 0.00266 cm/s for the fast, intermediate, and slow experiments, respectively. Interestingly, the intermediate experiment produced the largest fitted radial growth rate, suggesting that plume growth was not determined solely by the nominal injection rate.

On the whole, from the comparison made above, one can conclude that the injection rate is crucial for hydrogen plume formation, hydrogen trapping, mixing zone formation, and recovery.

Fast injection resulted in the biggest hydrogen plume and in the highest final recovery of hydrogen, whereas slow injection caused a small hydrogen plume and a small final recovery of hydrogen. On the contrary, the discrepancy between fitted hydrogen plume growth rates shows that the correlation between injection rate and hydrogen plume growth rate is not linear.

The information received in the laboratory work can become a basis for quantified analysis of hydrogen behavior during repeated injections and extractions. Further measurements of flow rate, repetition of the experiment, and hydrogen plume mapping in space will make possible the decrease of uncertainties in this experiment.

References

[1] Niklas Heinemann et al. "Enabling large-scale hydrogen storage in porous media – the scientific challenges". In: *Energy & Environmental Science* 14.2 (2021), pp. 853–864. DOI: 10.1039/D0EE03536J.

[2] Haval Kukha Hawez, Shaee Radha Omar, and Layla Lateef Alwan. "Underground Hydrogen Storage: A Comprehensive Review of Technologies, Geological Formations, and Future Prospects". In: *Energies* 19.12 (2026), p. 2760. DOI: 10.3390/en19122760.

[3] Maksim Lysyy et al. "Hydrogen Relative Permeability Hysteresis in Underground Storage". In: *Geophysical Research Letters* 49.17 (2022), e2022GL100364. DOI: 10.1029/2022GL100364.